RESEARCH ARTICLE

Key Points:
- Ocean response to Megi is relatively accurately simulated by the atmosphere-ocean coupled model
- Use of the coupled three-dimensional ocean model is critical to obtain accurate upper ocean response
- Stable boundary layer forms above cold SST area and increases the inflow angle of the surface wind

Correspondence to:
C.-C. Wu,
cwu@typhoon.as.ntu.edu.tw

Tropical cyclone-ocean interaction in Typhoon Megi (2010)—A synergy study based on ITOP observations and atmosphere-ocean coupled model simulations

Chun-Chieh Wu[1], Wei-Tsung Tu[1], Iam-Fei Pun[1], I-I. Lin[1], and Melinda S. Peng[2]

[1]Department of Atmospheric Sciences, National Taiwan University, Taipei, Taiwan, [2]Marine Meteorology Division, Naval Research Laboratory, Monterey, California, USA

Abstract A mesoscale model coupling the Weather Research and Forecasting model and the three-dimensional Price-Weller-Pinkel ocean model is used to investigate the dynamical ocean response to Megi (2010). It is found that Megi induces sea surface temperature (SST) cooling very differently in the Philippine Sea (PS) and the South China Sea (SCS). The results are compared to the in situ measurements from the Impact of Typhoons on the Ocean in the Pacific (ITOP) 2010 field experiment, satellite observations, and ocean analysis field from Eastern Asian Seas Ocean Nowcast/Forecast System of the U.S. Naval Research Laboratory. The uncoupled and coupled experiments simulate relatively accurately the track and intensity of Megi over PS; however, the simulated intensity of Megi over SCS varies significantly among the experiments. Only the experiment coupled with three-dimensional ocean processes, which generates rational SST cooling, reasonably simulates the storm intensity in SCS. Our results suggest that storm translation speed and upper ocean thermal structure are two main factors responsible for Megi's distinct different impact over PS and over SCS. In addition, it is shown that coupling with one-dimensional ocean process (i.e., only vertical mixing process) is not enough to provide sufficient ocean response, especially under slow translation speed (~2–3 m s^{-1}), during which vertical advection (or upwelling) is significant. Therefore, coupling with three-dimensional ocean processes is necessary and crucial for tropical cyclone forecasting. Finally, the simulation results show that the stable boundary layer forms on top of the Megi-induced cold SST area and increases the inflow angle of the surface wind.

1. Introduction

Track predictions of tropical cyclone (TC) have been significantly improved over the past three decades, yet progress in TC intensity forecasts has been limited. The internal dynamics, environmental forcing, and ocean features are generally identified as important elements affecting TC intensity change [*Wang and Wu*, 2004]. Specifically, in terms of TC intensification, certain ocean conditions, such as sea surface temperature (SST) and upper ocean thermal structure (UOTS; upper ocean typically means 0–200 m or so), play an important role [*Shay et al.*, 2000; *Lin et al.*, 2005; *Wu et al.*, 2007; *Jaimes et al.*, 2015; *Cione*, 2015]. A TC exerting strong wind stress on the ocean surface induces significant cooling in SST through the dynamic processes of entrainment mixing and upwelling [*Price*, 1981; *Price et al.*, 1994]. The major factors affecting the above dynamic processes are the TC translation speed and the underlying UOTS [*Price*, 1981; *Price et al.*, 1994; *Bender and Ginis*, 2000; *Wu et al.*, 2007; *Lin et al.*, 2008; *Yablonsky and Ginis*, 2009]. TC-induced SST cooling, in turn, has been considered one of the main factors that limit the storm intensity and its intensification. *Bender and Ginis* [2000] showed that forecasts of TC intensity could be significantly improved when the TC-induced ocean feedback was considered into the model simulations. In fact, UOTS is highly related to the ocean features (e.g., eddies), which can now be effectively detected from the sea surface height anomaly field observed by satellite altimetry [*Lin et al.*, 2005, 2008; *Goni et al.*, 2009]. The observational and numerical studies have shown that rapid intensification can occur when the storm passes over a warm ocean eddy. In contrast, when the TC encounters a cold ocean eddy, the SST cooling can be enhanced, and thus TC intensity would be further limited due to the stronger negative feedback associated with the decrease of the heat flux from the ocean [*Lin et al.*, 2005, 2008; *Wu et al.*, 2007; *Sung et al.*, 2014; *Walker et al.*, 2014]. Therefore, it is important to include the information of ocean eddies while conducting TC intensity forecasts.
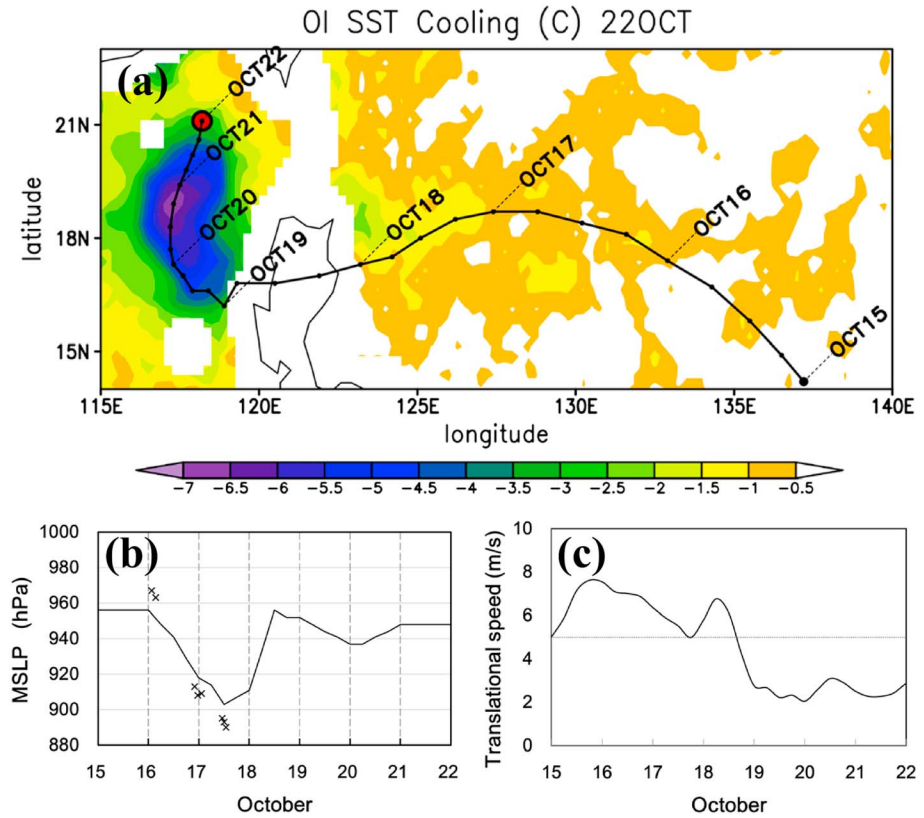
Figure 1. (a) Megi-induced SST cooling based on satellite SST observations between 22 October 2010 and 15 October 2010. Megi's track is superimposed. (b and c) Megi's 6-hourly minimum sea level pressure and translation speed from 0000 UTC 15 October to 0000 UTC 22 October 2010, respectively. The "crosses" in Figure 1b represent the observations from the C-130 aircrafts during the ITOP experiment. Megi's best-track data are from JTWC. The ocean response, i.e., SST cooling, is much significant over the SCS than over the PS.

Some recent studies [e.g., *Bender et al.*, 2007] suggested that coupling one-dimensional (1-D) ocean processes associated with the current shear-induced mixing in an ocean model is adequate to represent the TC-induced upper ocean responses. However, for a slow-moving TC or a TC that is over the ocean with relatively low upper ocean heat content, the three-dimensional (3-D) ocean processes cannot be neglected [*Price*, 1981; *Price et al.*, 1994; *Lin et al.*, 2005; *Yablonsky and Ginis*, 2009; *Halliwell et al.*, 2011]. Meanwhile, in a recent study, based on an atmosphere-ocean coupled model, *Lee and Chen* [2014] showed that the TC-induced cold wake affects not only TC intensity but also TC structure. Warm air over the cooler SST can enhance the stability of the TC boundary layer (TCBL) and result in the formation of a stable boundary layer (SBL). Thus, convection in rainbands would be suppressed, and the inflow angle would increase. The enhanced inflow allows the moisture-laden air of the boundary layer to enter the storm core with higher equivalent potential temperature and thus results in deeper convection in the inner core. The stabilizing effect can counteract and partially offset the negative feedback on intensity associated with the TC-induced cold wake.

The abundant atmospheric (e.g., dropsondes) and oceanic (e.g., Airborne Expendable BathyThermograph; AXBT) data obtained from aircrafts and research vessels during ITOP (Impact of Typhoons on the Ocean in the Pacific, 2010) field experiment [*D'Asaro et al.*, 2014; *Lin et al.*, 2013] provide a unique opportunity to further investigate the interaction between the TC and its underlying ocean. As a case in point, Typhoon Megi (2010), of which the evolution is shown in Figure 1, intensified rapidly and reached category 5 intensity at moderate TC translation speed (5–7 m s^{-1}) over the Philippine Sea (PS) associated with a favorable UOTS (i.e., the depth of 26°C isotherm ~ 110 m) [*Lin et al.*, 2013; *Ko et al.*, 2014]. The intensity of Megi decreased after making landfall in Luzon and then reintensified slightly after entering the South China Sea (SCS). During Megi's
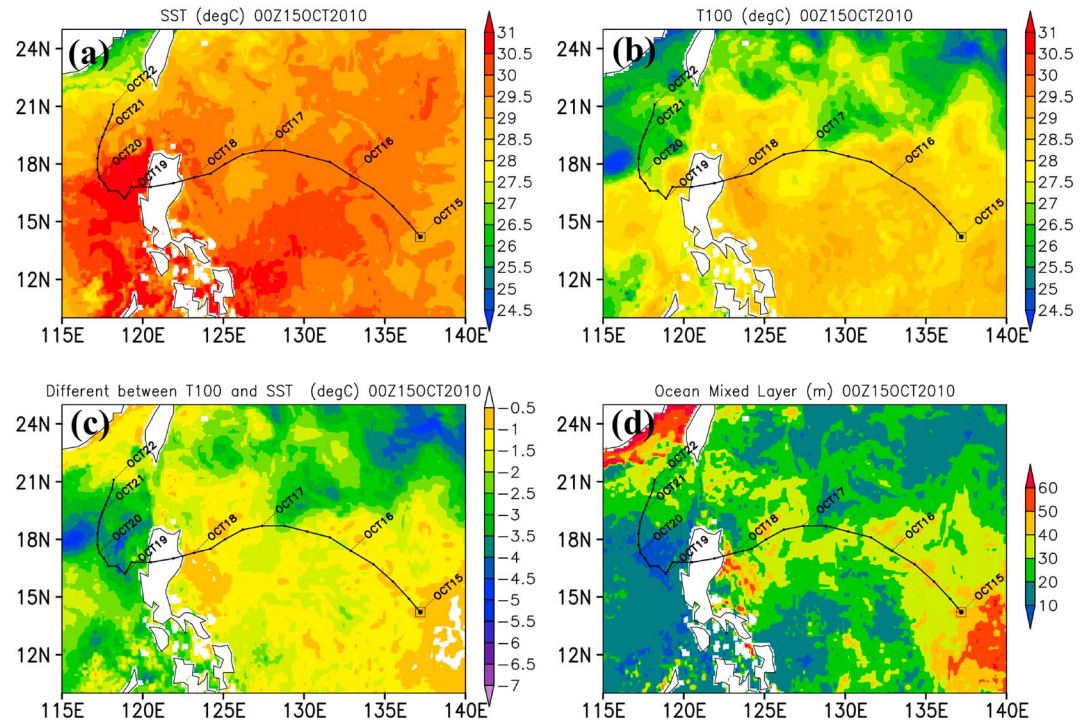
Figure 2. Initial ocean thermal condition for the experiments starting from 0000 UTC 15 October. (a) SST, (b) T100, (c) T100 minus SST, and (d) mixed layer depth. Megi's track is superimposed, and the open square depicts the initial location of Megi in the model simulations. The subsurface thermal structure is very different between the SCS and the PS (Figures 2b–2d), although both SSTs are relatively warm (Figure 2a).

passage over SCS, its track recurved sharply from westward to northward with slow TC translation speed (about $2.5\,\mathrm{m\,s}^{-1}$) and steady intensity.

In this study, huge contrast in Typhoon Megi's evolution between the two basins (PS versus SCS) is identified [cf. *D'Asaro et al.*, 2014; *Ko et al.*, 2014; *Guan et al.*, 2014]. By employing an atmosphere-ocean coupled model including either 1-D or 3-D ocean processes, this study investigates the ocean responses in these two basins and their impacts on Megi's intensity, as well as examines the role of SBL. The atmosphere-ocean coupled model and experiment designs are described in section 2. Section 3 presents the results from model simulations as well as the feature of SBL and its impact on Megi. Finally, the summary is given in section 4.

2. Model and Experiment Designs

2.1. Atmosphere-Ocean Coupled Model

The atmosphere-ocean coupled model employed in this study is based on the University of Miami Coupled Model [*Chen et al.*, 2007, 2013; *Lee and Chen*, 2014], which consists of the Weather Research and Forecasting Model (WRF) [*Skamarock et al.*, 2008] and the three-dimensional Price-Weller-Pinkel (3DPWP) ocean model [*Price et al.*, 1994]. The detail of coupling processes is described in *Lee and Chen* [2014]. The WRF and 3DPWP use the same time step which is set as 1 min in the outermost domain. The WRF model exchanges its information of the surface layer (e.g., surface wind stress) with that of the top layer in the 3DPWP at every time step.

In WRF, the horizontal grid points in the 12, 4, and 1.3 km domains are 334×250, 250×250, and 250×250, and the inner two domains are vortex-following movable nests while the outermost domain is fixed. The vertical grid points are 35 η levels with 8 levels in the lowest 1 km. The model physics contains the Kain-Fritsch scheme [*Kain*, 2004] for cumulus parameterization (only adopted in the outermost domain), the WRF single-moment six-class [*Hong and Lim*, 2006] scheme for microphysical parameterization,
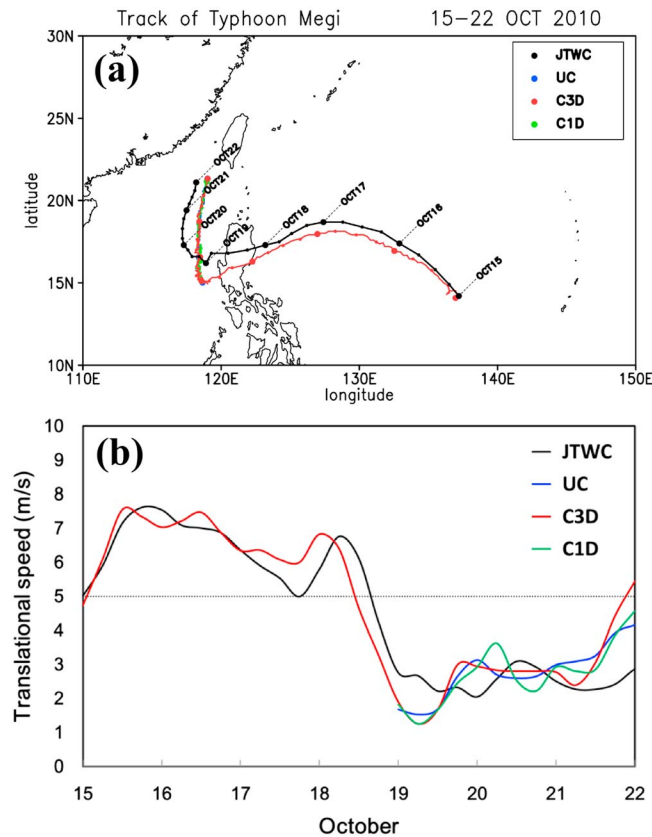
Figure 3. Model simulated (a) track and (b) translation speed of Megi from 0000 UTC 15 October to 0000 UTC 22 October 2010. In the PS segment, only C3D simulated results (red lines) are shown. Blue and green lines represent UC and C1D simulations. Differences in track simulations among all the experiments are small.

the Yonsei University [*Hong et al.*, 2006] scheme for the boundary layer parameterization, and the Monin-Obukhov scheme for the surface layer parameterization with the surface drag and enthalpy coefficient based on *Donelan et al.* [2004] and *Garratt* [1992], respectively.

The 3DPWP has the same horizontal grid points as in WRF and has 30 vertical layers with intervals of 10 m and 20 m for layers from 5 m (the top level in the 3DPWP and considered as the sea surface) to 195 m and from 210 m to 390 m, respectively. The ocean processes include entrainment/mixing, vertical advection/upwelling, horizontal advection, and pressure gradient force. However, it should be noted that the present implementation of the 3DPWP does not contain background ocean currents and bathymetry.

2.2. Experiment Designs

To investigate the ocean response to Megi, an uncoupled experiment (UC) and two coupled experiments are conducted here. The latter two are coupled with the 3-D ocean processes (C3D) and the 1-D ocean processes (C1D, which only considers vertical entrainment/mixing processes and does not include advection processes), respectively. Then we compare the results from the above three experiments to clarify the role of the ocean and the importance of 3-D ocean processes in TC simulations.

The limited ocean response (i.e., SST cooling = ~1°C) and the subsequent impact on Megi's intensity among all experiments in PS are similar (Figure 6a), suggesting that Megi is relatively insensitive to the underlying ocean processes, specifically when UOTS is favorable. Therefore, from the TC perspective, we focus on the SCS region where the ocean response is more pronounced and thus has a great impact on Megi's intensity. To further investigate the ocean response among all experiments in SCS without the influence of PS, we keep the intensity and structure of the simulated Megi identical before and after the typhoon passes over PS. Therefore, the C3D experiment is carried out for 4 days starting from 0000 UTC 15 October, and the model output of C3D at 0000 UTC 19 October is used as the initial condition for all experiments for the following 3 days of simulation, viz., the period during which Megi travels over SCS. This step ensures that the simulated Megi in all experiments is identical before entering SCS.

Final analysis data of the National Centers for Environmental Prediction is used as the initial and lateral boundary condition in WRF. The initial field (e.g., temperature and salinity) for the ocean model is based on the analysis data from the Hybrid Coordinate Ocean Model (HYCOM). However, the SST field in the HYCOM analysis is substituted with satellite microwave observations from the Tropical Rainfall Measuring Mission/Microwave Imager and Advanced Microwave Scanning Radiometer for Earth Observing System. It is found that the differences in the initial UOTS between PS and SCS are significant (Figure 2). Although the SST in PS is slightly colder than the SST in SCS, the subsurface thermal structure in PS appears more favorable for TC intensification as compared to that in SCS. It can be clearly seen that PS has higher T100
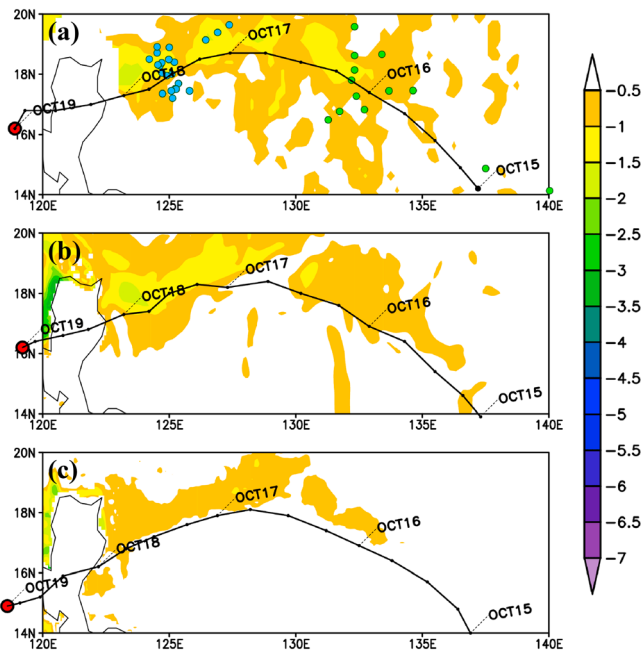
Figure 4. SST cooling at 0000 UTC 19 October 2010 relative to the initial SST 0000 UTC 15 October 2010 based on (a) satellite observations, (b) EASNFS, and (c) C3D simulation. The green (blue) dots in Figure 4a represent the AXBT drop off locations on 16 (17) October 2010 during the ITOP field experiment. Six-hourly JTWC best-track data are superimposed. The red dot indicates the center of Megi at 0000 UTC 19 October 2010. The cooling over the PS in the C3D simulation is consistent with the satellite observation and EASNFS analysis.

(the average temperature from surface to 100 m depth) [*Price*, 2009] and deeper ocean mixed layer depth (Figures 2b and 2d). Recall that in this study the initial (or background) current in the ocean model is set at rest and that the currents are generated through geostrophic adjustment. In fact, the background current should not make significant difference to the present results.

2.3. Eastern Asian Seas Nowcast/Forecast System

Because there is no AXBT observation during Megi's passage over SCS in the ITOP experiment, it is difficult to verify the results of the model simulations conducted in the present study. Collaborating with the U.S. Naval Research Laboratory (NRL), we use the data set from the Eastern Asian Seas Nowcast/Forecast System (EASNFS) [*Ko et al.*, 2008] for the comparison. EASNFS is based on the Navy Coastal Ocean Model. Better atmospheric forcing is derived from WRF. Assimilating the ITOP data (e.g., the location of TC center, storm motion vector, and the 700 hPa axisymmetric surface wind profile) based on the Ensemble Kalman Filter system

[*Wu et al.*, 2010], the forcing is then used to drive EASNFS to generate realistic ocean analysis field. In all, the ocean response in the model simulations can therefore be verified by both the satellite observation and the high temporal and spatial resolution ocean analysis from EASNFS.

3. Results and Discussions

3.1. The Tracks of the Simulated Megi

The intensities and tracks of the 7 day simulation starting from 0000 UTC 15 October in all experiments are similar, and the differences between the tracks of all experiments are less than 30 km (not shown). Some southward deviations (of about 100–150 km) are found at 48 h before Megi reaches Luzon (only the result of C3D is shown in Figure 3). The ocean response in C3D, such as the position of cold wake (on the right-hand side of the TC track) and the value of maximum SST cooling (of about 1.5°C), is close to the satellite observation and EASNFS ocean analysis (Figure 4). In addition, the vertical profile of the ocean temperature in C3D is consistent with the AXBT data from ITOP and their coefficient of determination (R^2) is up to 0.92 (Figure 5), though less correlation occurs in the upper 50 m. This lower correlation is probably due to a relative small range of temperature variation (~3°C) and the somewhat mismatch of cooling patterns between observations and model simulations (Figure 4). Nevertheless, the root-mean-square difference between simulated and observed temperatures in the upper 50 m is about 0.7°C, suggesting that the model is still of reasonable accuracy. According to the above results, it is adequate to consider the 4 day simulation of C3D as the prerun for all experiments in SCS.

In all 3 day simulations in SCS starting from 0000 UTC 19 October, the tracks of Megi are generally consistent with one another, as well as with the best track from Joint Typhoon Warning Center (JTWC, Figure 3). Although some eastward bias (of about 100–150 km) are found after Megi's departure from Luzon, all experiments can generally capture the feature of northward recurvature and rapid decrease of the TC translation
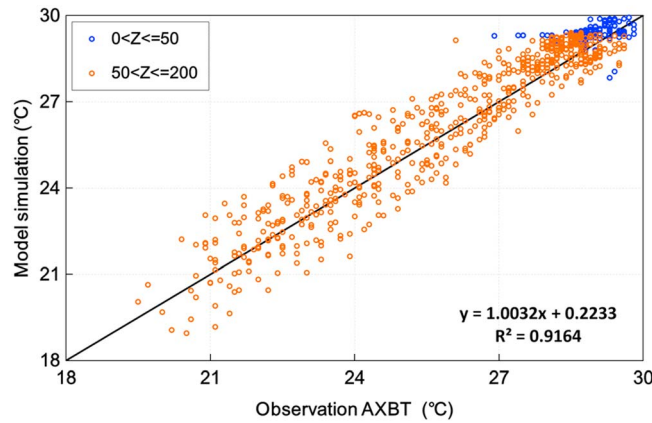
Figure 5. Comparison between AXBT observations and C3D simulations. Blue dots represent the data between surface and 50 m depth, while red dots represent the data between 50 and 200 m depth. The coefficient of determination (R^2) between observation and model is up to 0.92.

speed over SCS. The nearly identical tracks among all experiments indicate that the ocean has no significant impact on the motion of Megi over this relatively short (4 day) simulation period. In this paper, the focus is to examine the response of ocean to Megi and its feedback to Megi's intensity.

3.2. Megi's Evolutions and Ocean Responses Among Three Experiments

The evolutions of minimum sea level pressure (MSLP) in the uncoupled and coupled experiments (namely UC, C1D, and C3D) are shown in Figure 6. Although the simulated intensity in C3D is weaker than the best-track data of both JTWC and Japan Meteorological Agency (JMA) by about 20 hPa, the feature of rapid intensification can still be well simulated during the same period from 1200 UTC 16 October (965 hPa) to 1200 UTC 17 October (919 hPa). The simulated maximum intensity (908 hPa) is reached at 2000 UTC 17 October before making landfall in Luzon. Evolution of the simulated intensity is found to be relatively diverse after 0600 UTC 19 October over SCS. In the uncoupled experiment (UC), the storm continues to intensify and reaches a lower MSLP (903 hPa) at 1700 UTC 21 October than that over PS. However, the storm intensities in coupled experiments (C1D and C3D), both of which consider the ocean feedback, increase slowly and only reach an MSLP of 925 hPa and 931 hPa, respectively. These features can also be found in both best-track data sets. The discrepant evolution of storm intensity among these three experiments can clearly be attributed to the negative SST feedback, i.e., significant SST cooling in SCS, as observed by satellite (Figure 1a).

Data of the sea surface current in C1D, C3D, and EASNFS analyses are shown in Figure 7. The surface current induced by the wind stress of Megi in C3D remains on the right-hand side of the TC track and appears in a
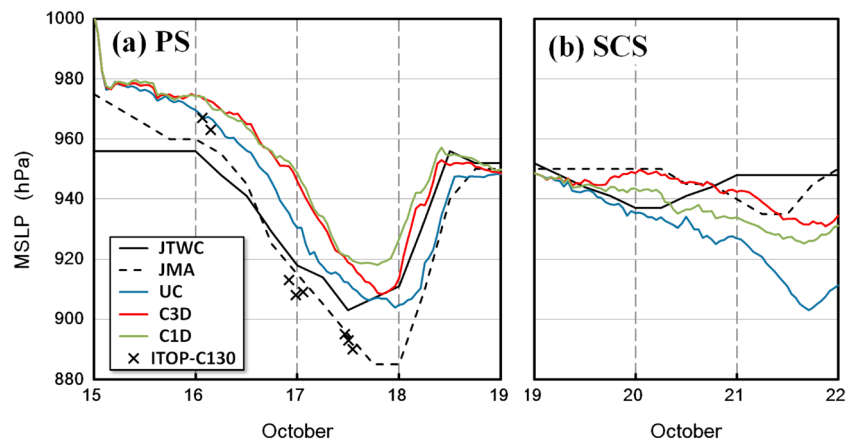

Figure 6. The evolutions of simulated and observed Megi intensity as defined by MSLP over (a) the PS and (b) the SCS. The initial condition in Figure 6a is from HYCOM analysis on 15 October 2010, whereas the initial condition in Figure 6b is from C3D output at 0000 UTC 19 October 2010. Blue, red, and green lines represent the simulations from UC, C3D, and C1D, respectively. Black solid and dashed lines represent the best-track data from JTWC and JMA, respectively. Crosses represent the observations from C-130 aircrafts during the ITOP experiment. The overall differences in the intensity evolution between coupled and uncoupled experiments are small over the PS, while becoming significant in the SCS due to different ocean responses.
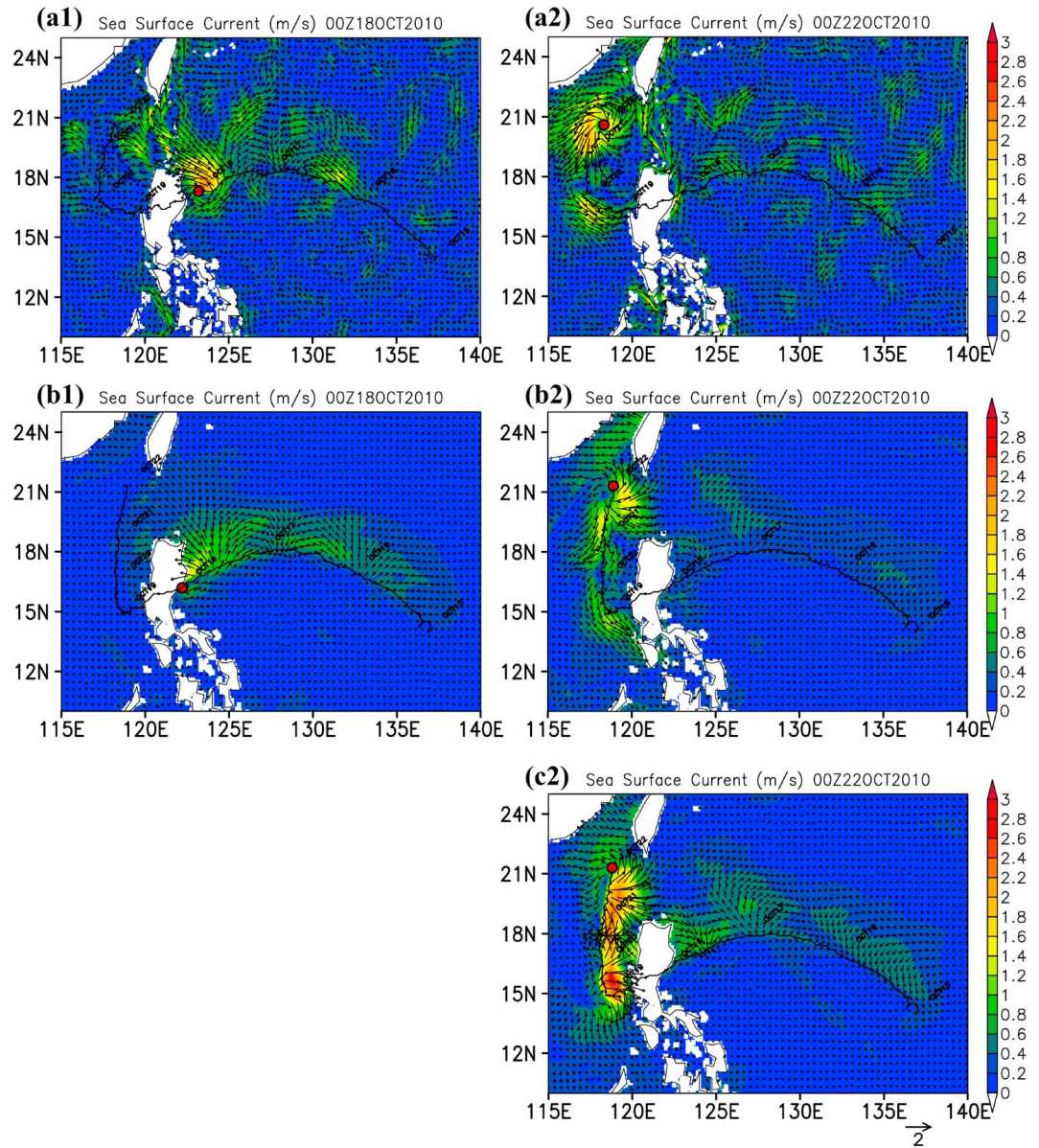
Figure 7. Sea surface current at (1) 0000 UTC 18 October and (2) 0000 UTC 22 October from (a) EASNFS ocean analysis, (b) C3D, and (c) C1D. Megi's track is superimposed, and the red dot represents the center of Megi on that day. Note that since C1D experiment starting from 0000 UTC 19 October, there is no sea surface current display at 0000 UTC 18 October.

clockwise near-inertial motion. Before 0000 UTC 18 October, the surface current over PS in C3D intensifies with the increasing storm intensity and reaches a current speed of $1.2\,\mathrm{m\,s^{-1}}$. Similar to C3D, the surface current in EASNFS occurs on the right-hand side of the TC track but reaches a slightly higher current speed of $1.8\,\mathrm{m\,s^{-1}}$ over PS. The simulated surface current of C3D over PS is relatively close to that of EASNFS. As Megi enters SCS during the period from 1800 UTC 18 October to 0300 UTC 19 October, the translation speed of Megi rapidly slows down prior to the sudden northward recurvature. Although the intensification of Megi over SCS is less significant than that over PS, the ocean response of the surface current of SCS in C3D is still clear due to the slow translation speed. The result of C3D, which simulates a surface current of about $1.8\,\mathrm{m\,s^{-1}}$ over SCS, is consistent with that of EASNFS, while the surface current of $2.8\,\mathrm{m\,s^{-1}}$ in C1D is apparently overestimated.
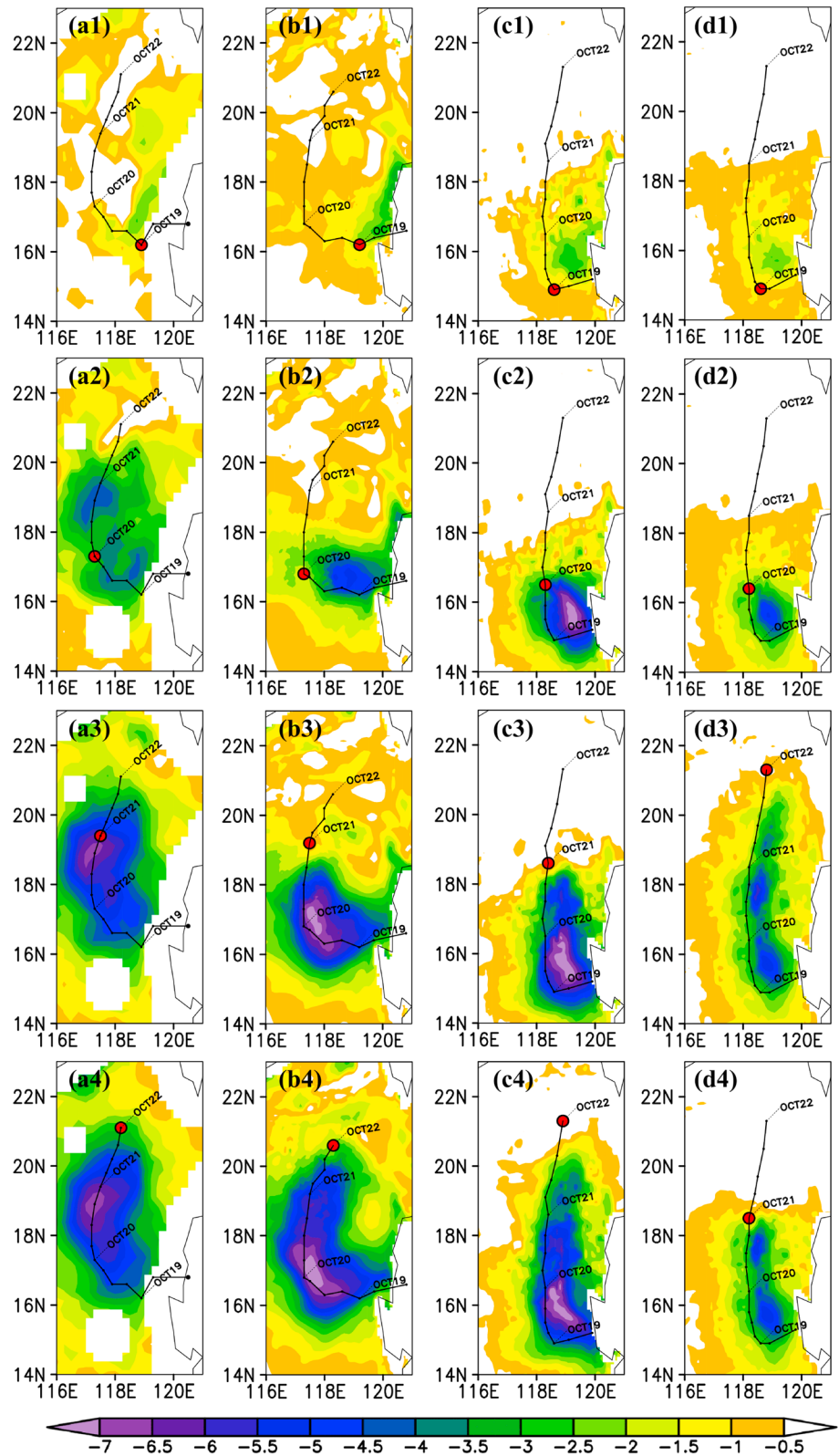
Figure 8. Megi-induced SST cooling in the SCS based on (a) satellite observation, (b) EASNFS, (c) C3D, and (d) C1D. SST cooling is estimated relative to the SST at 0000 UTC 15 October 2010. Rows (1) to (4) are the SST cooling at 0000 UTC from 19 to 22 October 2010. Six-hourly track of Megi is superimposed, and the red dot indicates the location of Megi on that day. EASNFS, C3D, and C1D are all able to capture the distribution of SST cooling, with the maximum cooling occurring at the recurvature point.
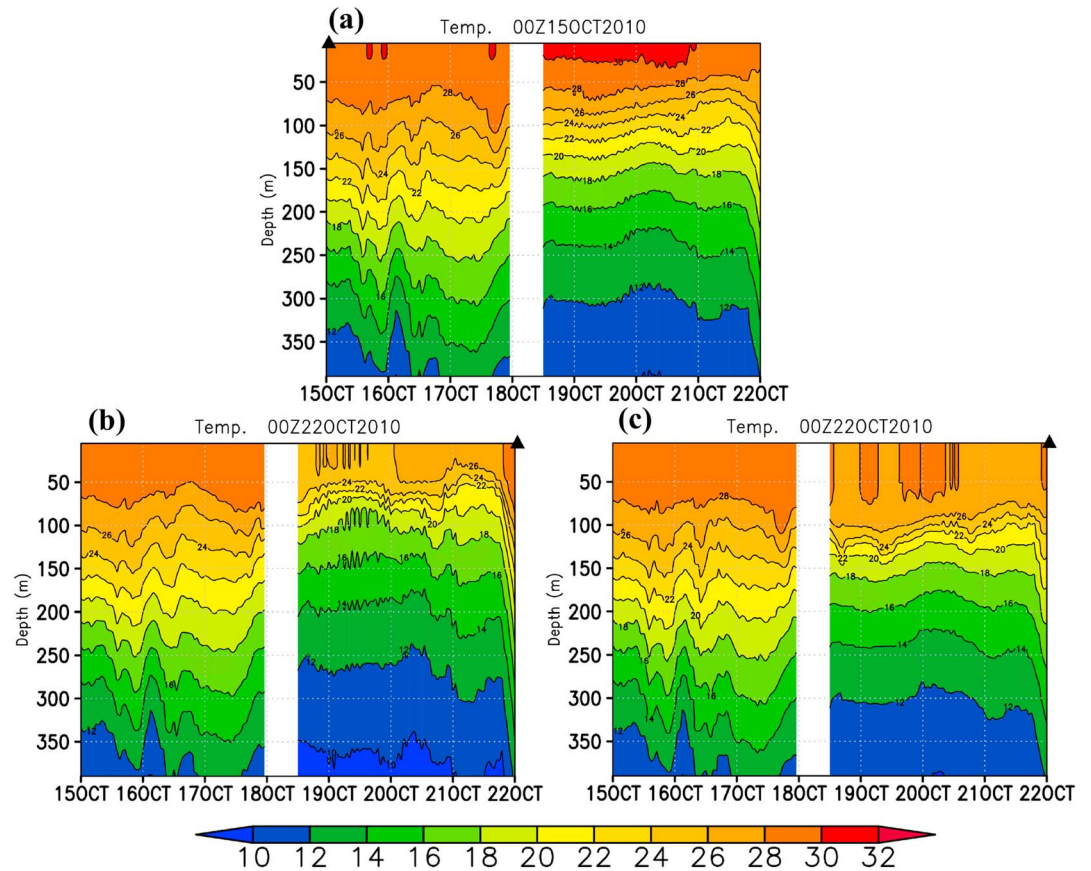
Figure 9. (a) Initial ocean thermal structure along Megi's track at 0000 UTC 15 October 2010. (b and c) Simulated ocean thermal structure at 0000 UTC 22 October 2010 from C3D and C1D, respectively. The triangle represents the location of Megi, and the white area represents the Luzon Island. The upper ocean responses between C3D and C1D are significantly different over the SCS (after 19 October 2010).

According to satellite observation (Figure 8a), the change in SST from 0000 UTC 19 October to 0000 UTC 22 October clearly appears along Megi's track with a pronounced SST cooling of about 7°C. C1D, C3D, and EASNFS are all able to capture the distribution of SST cooling, with the maximum cooling occurring at the turning point (Figures 8b–8d). Both ocean-coupled experiments (C1D and C3D) can simulate such ocean response, although the SST cooling in C1D only reaches about 5°C. Due to the absence of upwelling process in C1D, the SST cooling is underestimated and the degree of underestimation is affected by the TC translation speed and the underlying UOTS. In the C1D experiment starting at 0000 UTC 15 October (hereafter C1D_1015), the SST cooling over PS is similar to that in C3D (not shown) due to the favorable UOTS for TC development and the moderate TC translation speed ($5–7 \, \mathrm{m \, s}^{-1}$). In C1D, the underestimation in both magnitude and extent of SST cooling is relatively pronounced in SCS than that in PS due to the unfavorable UOTS for the storm intensification (i.e., thinner ocean mixed layer and lower T100, Figure 2) and slow TC translation speed (about $2.5 \, \mathrm{m \, s}^{-1}$, Figure 3b). This feature is consistent with the results from previous numerical studies [*Sanford et al.*, 2007; *Yablonsky and Ginis*, 2009; *Halliwell et al.*, 2011].

In addition to verifying the SST cooling of model simulations, it is necessary to assess the performance of the upper ocean evolution at different depths. As discussed in section 3.1, the AXBT data from ITOP is used to verify the ocean response of C3D over PS. Due to the absence of AXBT data over SCS, we employ the EASNFS analysis to verify the result of our simulations, in particular the vertical profile of ocean temperature over SCS. The along-track vertical profiles of ocean temperature in C1D and C3D are shown in Figure 9. At the initial state (Figure 9a), it is shown that the initial warm features of PS, including a thicker ocean mixed layer and weaker stratification below the ocean mixed layer, provide a more favorable ocean condition for Megi to reach category 5 intensity, despite the lower SST in PS than that in SCS. As Megi passes through both PS and
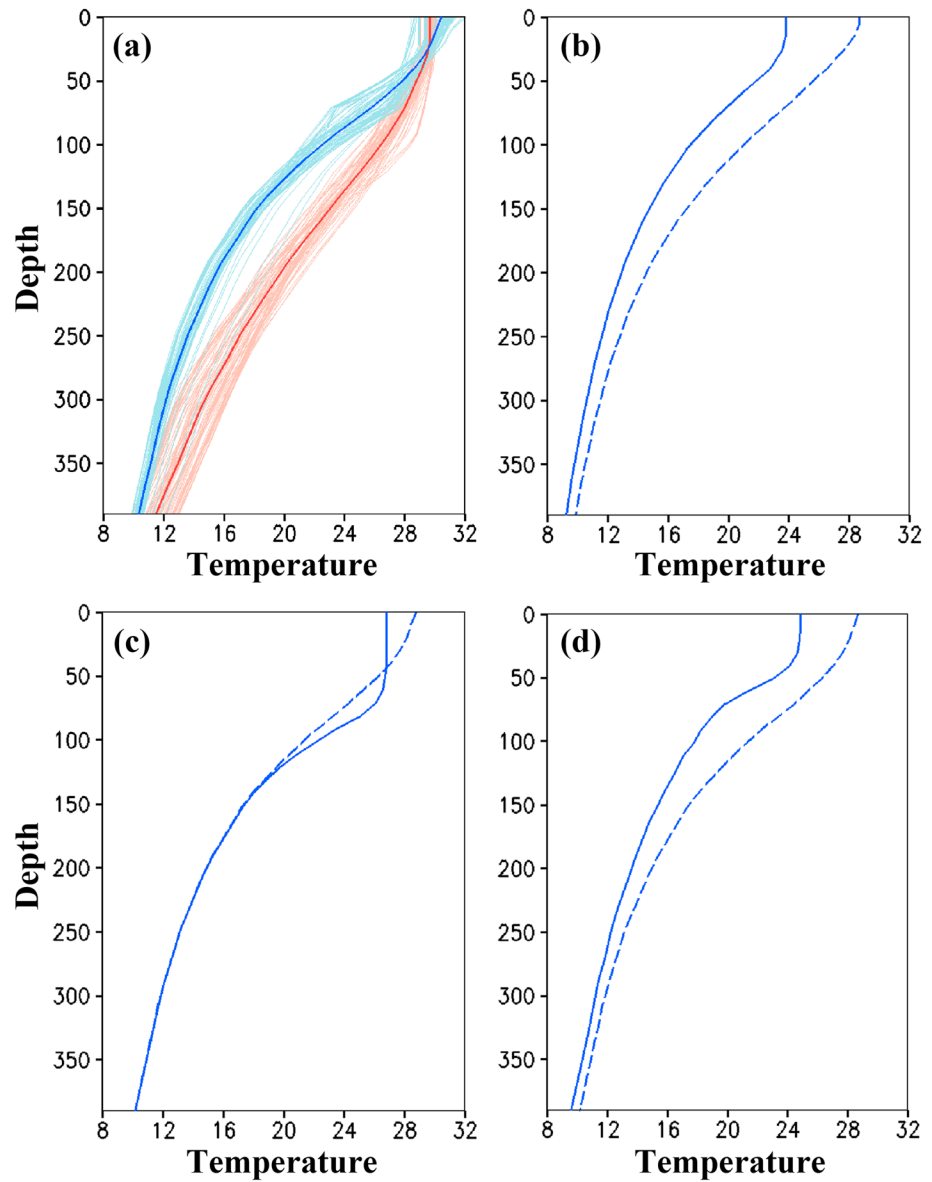
Figure 10. Profiles of averaged temperature along Megi's track. (a) Temperature profiles at the initial time 0000 UTC 15 October 2010. Thick (thin) lines represent averaged (individual) temperature profile, while red and blue ones depict profiles in PS and SCS, respectively. (b, c, and d) Averaged temperature profiles over the SCS segment from EASNFS, C1D, and C3D simulations at 0000 UTC 15 October 2010, respectively. The solid (dashed) line indicates time period after (before) Megi. The changes in the upper ocean thermal structure are similar between EASNFS and C3D.

SCS, the TC-induced upper ocean responses in PS and in SCS are significantly different (Figures 9b and 9c). In PS, the result of C3D indicates that the change of upper ocean temperature is small, and that there is a similar result in C1D_1015 (starting at 0000 UTC 15 October) (Figure 9). The vertical profiles of ocean temperature in SCS are significantly affected both in C3D and in C1D. It is found that in the former, the profile is shifted upward and the depth of ocean mixed layer is reduced due to the effect of upwelling process. As a result, C3D induces greater SST cooling as compared to the C1D experiment.

To clearly examine the difference of initial UOTS between PS and SCS, we average the along-track vertical profiles of ocean temperature in these two basins (Figure 10a). Since the SST in PS is about 30°C and close to that in SCS at the initial state, the storm intensity in UC, which does not consider SST negative feedback, increases both in PS and SCS (Figure 6). However, the difference in the initial UOTS between PS and SCS is
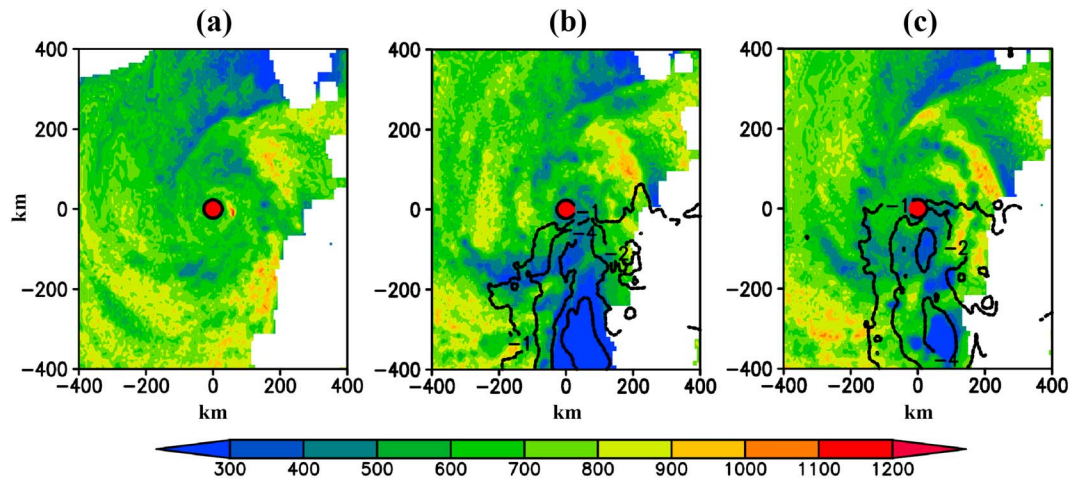
Figure 11. Simulated height of the TCBL (in meter) at 0000 UTC 21 October 2010 from (a) UC, (b) C3D, and (c) C1D. Contours represent the SST cooling, and the red dot indicates the center of Megi. The horizontal distributions of TCBL in C1D and C3D are similar to that in UC except over the cold wake region.

distinct and can cause significantly different ocean response with respect to varied ocean dynamic processes. The UOTS response in SCS is examined as follows. At 0000 UTC 22 October, the ocean mixed layer in C1D is deepened by the solely vertical mixing process, the upper ocean mixed layer is cooled and the lower ocean mixed layer is warmed through the vertical mixing of ocean temperature (Figure 10c). Due to the absence of advection processes and pressure gradient force in C1D, the ocean depth affected by the storm (of about 150 m) is limited. In C3D, the ocean temperature profile can be shifted upward by the upwelling process, and therefore, the colder water at deeper depth is carried upward (Figure 10d) (the temperature budget analysis shows that, as compared to the upwelling term, the other two terms from horizontal advection and pressure gradient force play rather minor roles in SST cooling (figures not shown)). The UOTS response of SCS in C3D is similar to that of EASNFS (Figures 10b and 10d). It is indicated that consideration of the 3-D ocean dynamic processes, particularly under an unfavorable ocean condition for storm intensification and/or a slow TC translation speed, can better capture the upper ocean response than considering only the vertical mixing process (i.e., C1D).

3.3. Stable Boundary Layer

Zhang et al. [2011] evaluated the impact of different definitions of TCBL from both dynamical and thermodynamical perspectives. Following the definition in *Lee and Chen* [2014], the TCBL in this study is defined as the
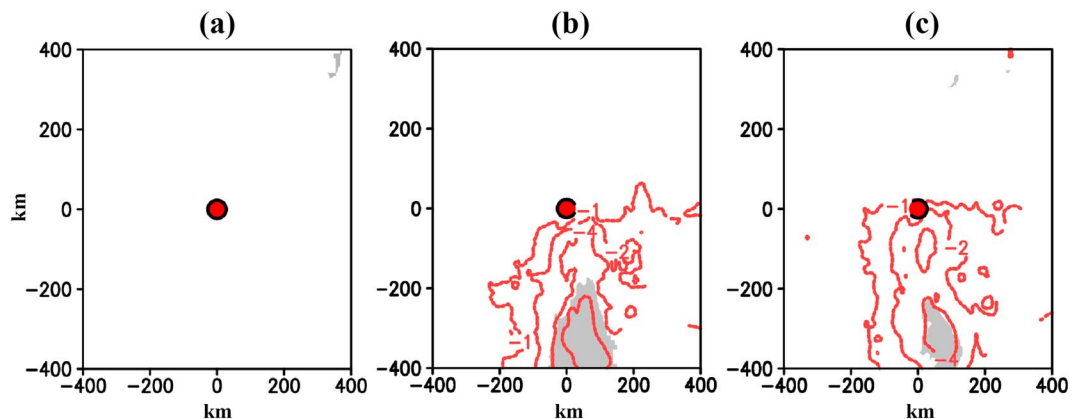
Figure 12. Same as Figure 11 but is for SBL (grey area). SBL forms over the area with strong Megi-induced SST cooling.
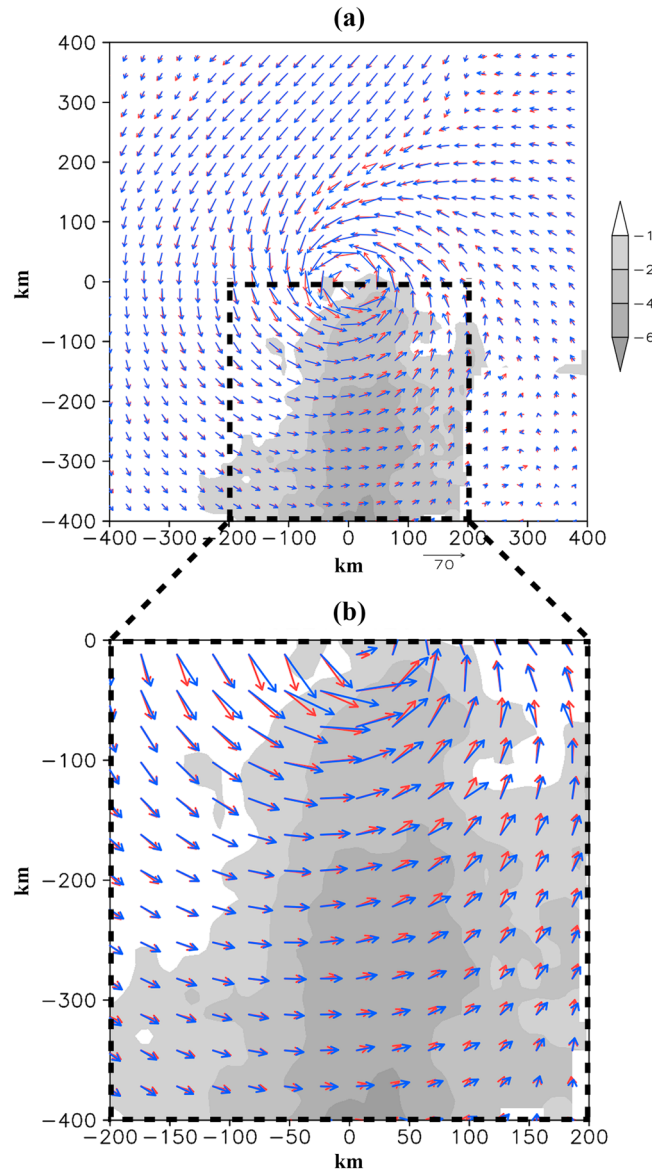
Figure 13. (a) Comparison of the wind fields between UC (blue) and C3D (red) at 0000 UTC 21 October 2010. The grey shading represents area of the SST cooling. (b) Zoom-in area over the SST cooling. The inflow angle of C3D in the cold wake region is larger than that of UC.

height at which the virtual potential temperature (θ_v) is 0.5 K higher than that at the surface. The horizontal distributions of TCBL height in UC, C1D, and C3D at 0000 UTC 21 October are shown in Figure 11. The height of TCBL in UC is about 600 m in the inner core region and about 800–1000 m in the outer region, and the horizontal distributions of TCBL in C1D and C3D are similar to that in UC except over the cold wake region. However, the height of TCBL in C1D and C3D is lower than 400 m in the pronounced cold wake region where the magnitude of SST cooling is less than 4°C. In particular, the height of TCBL in C3D is reduced to below 300 m. It is indicated that the height of TCBL is significantly reduced in the region where Megi has passed due to the TC-induced SST cooling. The stability of TCBL is also affected by the SST cooling effect.

In order to assess the effect of SST cooling, the stability of TCBL is defined by the sign of $\delta\theta_v/\delta z$ (i.e., stable for $\delta\theta_v/\delta z > 0$) [*Lee and Chen*, 2014]. We calculate the stability at each layer within the TCBL, which is referred as stable boundary layer (SBL) when all layers within TCBL are stable. The horizontal distributions of SBL in UC, C1D, and C3D at 0000 UTC 21 October are shown in Figure 12. While the SBL in UC is not formed, it is found that the features of SBL in C1D and C3D are evident, and especially more significant in C3D. Compared to Figures 11b and 11c, the region of SBL formation in Figure 12 is close to the region w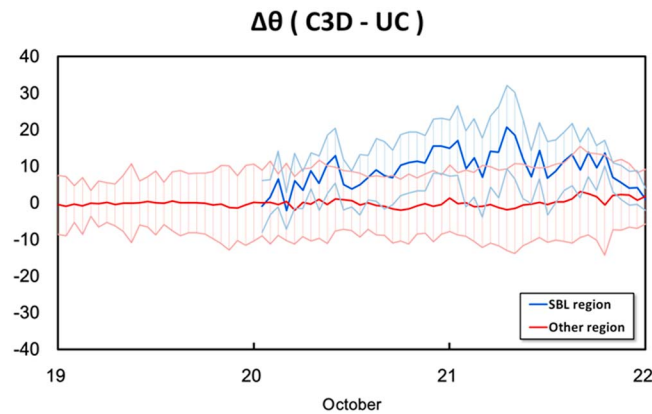here the height of TCBL is significantly reduced. It is found that consideration of the SST negative feedback not only reduces the height of TCBL but also increases its stability and forms the SBL.

To compare our results with those in *Lee and Chen* [2014], in this study we also examine the inflow angle which is defined as the angle between the actual wind and the tangential wind. To compare the difference of the inflow angle (10 m wind) between UC and C3D, the simulated Megi is relocated at the same center (Figure 13). Note that the TC translation speed is also deducted to remove the TC-movement-induced wave number 1 asymmetry. It is shown that the inflow angle of C3D in the cold wake region is larger than that of UC, but this feature is indistinct out of the cold wake region. To quantitatively evaluate the enhancement of inflow angle associated with the SBL effect induced by SST negative feedback, we calculate the area mean of the differences of inflow angle (C3D minus UC) within the radius between 150 and 400 km (excluding the inner core region where the calculated angle appears very sensitive to the high wind) in the SBL region and the other (non-SBL) region (Figure 14).

Figure 14. Difference in averaged inflow angle at 10 m within 150–400 km from Megi's center between C3D and UC. Blue and red colors represent such difference over SBL region and other (i.e., non-SBL) region, respectively. One standard deviation for each averaged line is shown. The unit is in degree.

It should be noted that SBL in C3D is formed at 0000 UTC 20 October. The fact that the mean difference of inflow angle is rather negligible in the other region without SBL indicates that the mean inflow angles in UC and in C3D are similar. In the SBL region, however, the mean difference of inflow angle is always positive (with the maximum up to 30°), i.e., the mean inflow angle of C3D in the SBL region is larger than that of UC due to the effect of SST cooling. The result from the above analysis is consistent with that in *Lee and Chen* [2014]. In order to discuss the significance of the result, the standard deviation is superposed, as indicated by the light-colored lines of Figure 14. Although the standard deviation in the SBL region overlaps with that in the other region, the mean difference of inflow angle in the SBL region including the standard deviation is largely positive. The enhancement of inflow angle induced by the SST cooling effect is statistically significant at the 99% confidence level (paired t test with one-sided distribution) [*Larsen and Marx*, 1981] during the period between 0000 UTC 20 October and 0000 UTC 22 October.

4. Summary

Based on the WRF-3DPWP coupled model, the ocean-uncoupled and ocean-coupled experiments are conducted in this case study of Megi (2010) to evaluate the impact of ocean dynamic process on the upper ocean thermal structure and the storm intensity. With the abundant atmospheric and ocean data from ITOP (2010), the results of model simulations can be verified through comparison with observations, including the AXBT in situ measurement, the satellite observation, and the EASNFS ocean analysis obtained from NRL.

In this study, an ocean-uncoupled experiment (UC) and two ocean-coupled experiments (C1D and C3D) with different ocean dynamic processes are conducted to evaluate the ocean responses and their impacts on Typhoon Megi. The comparison of results from UC, C1D, and C3D shows that all three experiments can capture Megi's track, and that the two ocean-coupled experiments can better simulate the evolution of Megi's intensity while the storm intensity in SCS is significantly overestimated in the ocean-uncoupled experiment. Overestimation of the storm intensity due to the lack of negative SST feedback is more significant for cases in which upper ocean thermal structure is more unfavorable for storm intensification, e.g., with shallower ocean mixed layer depth, lower ocean heat content, and slower TC translation speed.

It is found that a model coupled with 3-D ocean clearly outperforms the one coupled with 1-D ocean in generating appropriate ocean response, namely, SST cooling. This suggests that consideration of not only 1-D vertical mixing process but also 3-D (especially vertical) advection is critical to the success of TC intensity simulations, and thus of TC forecasts. These results are consistent with the previous numerical studies in the Atlantic basin [*Sanford et al.*, 2007; *Yablonsky and Ginis*, 2009; *Halliwell et al.*, 2011]. For typhoon main development region in the western North Pacific, typically only 30–40% of the ocean area appears to be favorable to TCs [*Pun et al.*, 2013], and statistically about 50% of typhoons have translation speed lower than 5 m s^{-1} [*Lin et al.*, 2014]. Therefore, consideration of a 3-D ocean model is crucial and would improve TC intensity simulations and forecasts in the western North Pacific.

Finally, the simulation results show that the stability of Megi's boundary layer has a close connection to its induced SST cooling. Stable boundary layer (SBL) forms above the cooling area, leading to an increase in inflow angle of 10 m winds and thus possibly affecting the inner core dynamics. The impact of SBL on Megi's intensity needs to be further investigated and is the topic of our next study.

List of Acronyms

3DPWP	Three-Dimensional Price-Weller-Pinkel
AXBT	Airborne Expendable BathyThermograph
C1D	Coupled one-dimensional ocean experiment
C1D_1015	Coupled one-dimensional ocean experiment starting at 0000 UTC 15 October
C3D	Coupled three-dimensional ocean experiment
EASNFS	Eastern Asian Seas Nowcast/Forecast System
HYCOM	Hybrid Coordinate Ocean Model
ITOP	Impact of Typhoons on the Ocean in the Pacific
JMA	Japan Meteorological Agency
JTWC	Joint Typhoon Warning Center
MSLP	Minimum Sea Level Pressure
NRL	Naval Research Laboratory
PS	Philippine Sea
SBL	Stable Boundary Layer
SCS	South China Sea
SST	Sea Surface Temperature
TC	Tropical Cyclone
TCBL	Tropical Cyclone Boundary Layer
UC	Uncoupled Experiment
UOTS	Upper Ocean Thermal Structure
WRF	Weather Research and Forecasting Model

References

Bender, M. A., and I. Ginis (2000), Real-case simulations of hurricane-ocean interaction using a high-resolution coupled model: Effects on hurricane intensity, *Mon. Weather Rev.*, *128*, 917–946.

Bender, M. A., I. Ginis, R. Tuleya, B. Thomas, and T. Marchok (2007), The operational GFDL hurricane-ocean prediction system and a summary of its performance, *Mon. Weather Rev.*, *135*, 3965–3989.

Chen, S. S., W. Zhao, M. A. Donelan, J. F. Price, and E. J. Walsh (2007), The CBLAST-Hurricane program and the next-generation fully coupled atmosphere-wave-ocean models for hurricane research and prediction, *Bull. Am. Meteorol. Soc.*, *88*, 311–317, doi:10.1175/BAMS-88-3-311.

Chen, S. S., W. Zhao, M. A. Donelan, and H. L. Tolman (2013), Directional wind-wave coupling in fully coupled atmosphere-wave-ocean models: Results from CBLAST-hurricane, *J. Atmos. Sci.*, *70*, 3198–3215, doi:10.1175/JAS-D-12-0157.1.

Cione, J. J. (2015), The relative roles of the ocean and atmosphere as revealed by buoy air-sea observations in hurricanes, *Mon. Weather Rev.*, *143*, 904–913.

D'Asaro, E., et al. (2014), Impact of typhoons on the ocean in the Pacific: ITOP, *Bull. Am. Meteorol. Soc.*, *95*, 1405–1418.

Donelan, M. A., B. K. Haus, N. Reul, W. J. Plant, M. Stiassnie, H. C. Graber, O. B. Brown, and E. S. Saltzman (2004), On the limiting aerodynamic roughness of the ocean in very strong winds, *Geophys. Res. Lett.*, *31*, L18306, doi:10.1029/2004GL019460.

Garratt, J. R. (1992), *The Atmosphere Boundary Layer*, 316 pp., Cambridge Univ. Press, New York.

Goni, G., et al. (2009), Applications of satellite-derived ocean measurements to tropical cyclone intensity forecasting, *Oceanography*, *22*, 190–197.

Guan, S., W. Zhao, J. Huthnance, J. Tian, and J. Wang (2014), Observed upper ocean response to typhoon Megi (2010) in the Northern South China Sea, *J. Geophys. Res. Oceans*, *119*, 3134–3157, doi:10.1002/2013JC009661.

Halliwell, G. R., Jr., L. K. Shay, J. K. Brewster, and W. J. Teague (2011), Evaluation and sensitivity analysis of an ocean model response to Hurricane Ivan, *Mon. Weather Rev.*, *139*, 921–945.

Hong, S.-Y., and J.-O. J. Lim (2006), The WRF single-moment 6-class microphysics scheme (WSM6), *J. Korean Meteorol. Soc.*, *42*, 129–151.

Hong, S.-Y., Y. Noh, and J. Dudhia (2006), A new vertical diffusion package with an explicit treatment of entrainment processes, *Mon. Weather Rev.*, *134*, 2318–2341.

Jaimes, B., L. K. Shay, and E. W. Uhlhorn (2015), Enthalpy and momentum fluxes during hurricane Earl relative to underlying ocean features, *Mon. Weather Rev.*, *143*, 111–131.

Kain, J. S. (2004), The Kain-Fritsch convective parameterization: An update, *J. Appl. Meteorol.*, *43*, 170–181.

Ko, D.-S., P. J. Martin, C. D. Rowley, and R. H. Preller (2008), A real-time coastal ocean prediction experiment for MREA04, *J. Mar. Syst.*, *69*, 17–28.

Ko, D.-S., S.-Y. Chao, C.-C. Wu, and I-I. Lin (2014), Impacts of typhoon Megi (2010) on the South China Sea, *J. Geophys. Res. Oceans*, *119*, 4474–4489, doi:10.1002/2013JC009785.

Larsen, R. J., and M. L. Marx (1981), *An Introduction to Mathematical Statistics and Its Applications*, 530 pp., Prentice-Hall, Inc, Englewood Cliffs, N. J.

Lee, C.-Y., and S. S. Chen (2014), Stable boundary layer and its impact on tropical cyclone structure in a coupled atmosphere-ocean model, *Mon. Weather Rev.*, *142*, 1927–1944.

Lin, I-I., C.-C. Wu, K. A. Emanuel, I-H. Lee, C.-R. Wu, and I. F. Pun (2005), The interaction of supertyphoon Maemi (2003) with a warm ocean eddy, *Mon. Weather Rev.*, *133*, 2635–2649.

Lin, I-I., C.-C. Wu, I.-F. Pun, and D.-S. Ko (2008), Upper-ocean thermal structure and the western North Pacific category 5 typhoons. Part I: Ocean features and the category 5 typhoons' intensification, *Mon. Weather Rev.*, *136*, 3288–3306.

Lin, I-I., P. Black, J. F. Price, C.-Y. Yang, S. S. Chen, C.-C. Lien, P. Harr, N.-H. Chi, C.-C. Wu, and E. A. D'Asaro (2013), An ocean coupling potential intensity index for tropical cyclones, *Geophys. Res. Lett.*, *40*, 1878–1882, doi:10.1002/grl.50091.

Lin, I-I., I. F. Pun, and C.-C. Lien (2014), "Category-6" supertyphoon Haiyan in global warming hiatus: Contribution from subsurface ocean warming, *Geophys. Res. Lett.*, *41*, 8547–8553, doi:10.1002/2014GL061281.

Price, J. F. (1981), Upper ocean response to a hurricane, *J. Phys. Oceanogr.*, *11*, 153–175.

Price, J. F. (2009), Metrics of hurricane-ocean interaction: Vertically-integrated or vertically-averaged ocean temperature?, *Ocean Sci.*, *5*, 351–368.

Price, J. F., T. B. Sanford, and G. Z. Forristall (1994), Forced stage response to a moving hurricane, *J. Phys. Oceanogr.*, *24*, 233–260.

Pun, I. F., I-I. Lin, and M.-H. Lo (2013), Recent increase in high tropical cyclone heat potential area in the Western North Pacific Ocean, *Geophys. Res. Lett.*, *40*, 4680–4684, doi:10.1002/grl.50548.

Sanford, T., J. Price, J. Girton, and D. Webb (2007), Highly resolved observations and simulations of the ocean response to a hurricane, *Geophys. Res. Lett.*, *34*, L13604, doi:10.1029/2007GL029679.

Shay, L. K., G. J. Goni, and P. G. Black (2000), Effects of a warm oceanic feature on Hurricane Opal, *Mon. Weather Rev.*, *128*, 1366–1383.

Skamarock, W. C., J. B. Klemp, J. Dudhia, D. O. Gill, D. M. Barker, M. G. Duda, X.-Y. Huang, W. Wang, and J. G. Powers (2008), A description of the Advanced Research WRF version 3, NCAR Tech. Note 475.

Sung, S.-L., C.-C. Wu, I-I. Lin, S.-S. Chen, and C.-Y. Lee (2014), Tropical cyclone-ocean interaction in Typhoon Fanapi (2010)—A synergy study based on ITOP observations, EnKF data assimilation, and coupled atmosphere-ocean models, "31st Conference on Hurricanes and Tropical Meteorology", Am. Meteorol. Soc., San Diego, Calif., March 31–April 4.

Walker, N. D., R. R. Leben, C. T. Pilley, M. Shannon, D. C. Herndon, I. F. Pun, I. I. Lin, and C. L. Gentemann (2014), Slow translation speed causes rapid collapse of northeast Pacific Hurricane Kenneth over cold core eddy, *Geophys. Res. Lett.*, *41*, 7595–7601, doi:10.1002/2014GL061584.

Wang, Y., and C.-C. Wu (2004), Current understanding of tropical cyclone structure and intensity changes—A review, *Meteorol. Atmos. Phys.*, *87*, 257–278.

Wu, C.-C., C.-Y. Lee, and I-I. Lin (2007), The effect of the ocean eddy on tropical cyclone intensity, *J. Atmos. Sci.*, *64*, 3562–3578.

Wu, C.-C., G.-Y. Lien, J.-H. Chen, and F. Zhang (2010), Assimilation of tropical cyclone track and structure based on the Ensemble Kalman Filter (EnKF), *J. Atmos. Sci.*, *67*, 3806–3822.

Yablonsky, R. M., and I. Ginis (2009), Limitation of one-dimensional ocean models for coupled hurricane-ocean model forecasts, *Mon. Weather Rev.*, *137*, 4410–4419.

Zhang, J. A., R. F. Rogers, D. S. Nolan, and F. D. Marks Jr. (2011), On the characteristic height scales of the hurricane boundary layer, *Mon. Weather Rev.*, *139*, 2523–2535.